

# RSNet: A Light Framework for The Detection of Multi-scale Remote Sensing Targets

Hongyu Chen<sup>✉</sup>, Chengcheng Chen<sup>✉</sup>, *Graduate Student Member, IEEE*,

Fei Wang<sup>✉</sup>, Yuhu Shi<sup>✉</sup>, Weiming Zeng<sup>✉</sup>, *Senior Member, IEEE*,

**Abstract**—Recent developments in synthetic aperture radar (SAR) ship detection have seen deep learning techniques achieve remarkable progress in accuracy and speed. However, the detection of small targets against complex backgrounds remains a significant challenge. To tackle these difficulties, this letter presents RSNet, a lightweight framework aimed at enhancing ship detection capabilities in SAR imagery. RSNet features the Waveletpool-ContextGuided (WCG) backbone for enhanced accuracy with fewer parameters, and the Waveletpool-StarFusion (WSF) head for efficient parameter reduction. Additionally, a Lightweight-Shared (LS) module minimizes the detection head's parameter load. Experiments on the SAR Ship Detection Dataset (SSDD) and High-Resolution SAR Image Dataset (HRSID) demonstrate that RSNet achieves a strong balance between lightweight design and detection performance, surpassing many state-of-the-art detectors, reaching 72.5% and 67.6% in mAP<sub>.50:95</sub> respectively with 1.49M parameters. Our code will be released soon.

**Index Terms**—Synthetic aperture radar (SAR), target detection, lightweight model, multiscale feature fusion

## I. INTRODUCTION

**S**YNTHETIC Aperture Radar (SAR) imagery is a vital tool in remote sensing [1], offering high-resolution images under all weather and lighting conditions. By using microwave signals that can penetrate atmospheric obstacles like clouds and rain, SAR provides detailed insights into terrain [2], vegetation [3], and man-made structures [4]. Its applications span geological exploration [5], disaster monitoring [6], agriculture [7], and urban planning. Notably, SAR excels in ocean monitoring [8], detecting subtle surface deformations, and generating digital elevation models, making it indispensable for modern earth observation.

As SAR image data scale and complexity increase, traditional image processing methods are becoming insufficient [9]. Recent advances in convolutional neural networks (CNNs) and Transformer architectures have significantly improved target detection [10], [11]. These deep learning methods are generally categorized into candidate region-based and regression-based approaches, with the latter excelling in real-time detection by directly regressing targets at multiple scales. For airborne SAR detection, one-stage methods strike a promising

balance between speed and accuracy; however, due to the computational and energy limitations of airborne platforms, a lightweight model framework is essential for practical deployment.

Building on the established model framework, several notable improvements have been proposed. For example, Tian et al. [12] introduced LFER-Net, which integrates SPDCConv and InceptionDWConv for high accuracy and efficiency. Zhou et al. [13] proposed HRLE-SARDet, leveraging hybrid representation learning to improve speed-accuracy balance. Chang et al. [14] presented MLSDNet, utilizing Adaptive Scale Distribution Attention (ASA) to enhance generalization and detection precision. Feng et al. [15] developed LPEDet, an anchor-free SAR ship detection model with a novel position-enhanced attention strategy. Yang et al. [16] designed a lightweight network featuring bidirectional pyramidal structures and soft quantization to minimize accuracy loss and background interference.

While advancements have shown the viability of lightweight models for SAR detection, substantial improvement opportunities remain. SAR images, unlike optical images, are prone to speckle noise, which reduces detail resolution [1], and face increased interpretation complexity due to geometric distortions. Furthermore, the processing of grayscale SAR data lacks intuitive color information. These factors hinder the balance between accuracy and detection speed, particularly regarding the crucial metric mAP<sub>.50:95</sub> for optimizing detection performance.

To tackle challenges in remote sensing image detection, we present RSNet, an optimized network based on YOLOv8, featuring improvements to its backbone, neck, and head. The backbone incorporates the Waveletpool-ContextGuided (WCG) structure, while the head employs the Waveletpool-StarFusion (WSF) network. Additionally, a Lightweight-Shared (LS) module in the detection head reduces the model's parameter load.

The primary contributions of this article are as follows:

- We developed the Waveletpool-ContextGuided (WCG) architecture, enhancing detection accuracy through anti-aliasing and contextual integration, achieving superior performance with fewer parameters.
- The Waveletpool-StarFusion (WSF) network employs wavelet upsampling pooling and starnet convolution layers, significantly reducing parameters while maintaining computational efficiency.

This work was supported by The National Natural Science Foundation of China [grant number 31870979]. (Corresponding author: Weiming Zeng)

Hongyu Chen, Chengcheng Chen, Fei Wang, Yuhu Shi, Weiming Zeng are with the Laboratory of Digital Image and Intelligent Computation, Shanghai Maritime University, Shanghai 201306, China (e-mail: hongychen676@gmail.com, shmtu\_ccc@163.com, shine\_wxf@163.com, syhustb2011@163.com, 1zengwm86@163.com).

Manuscript received XX, XXXX; revised XXXX XX, XXXX.

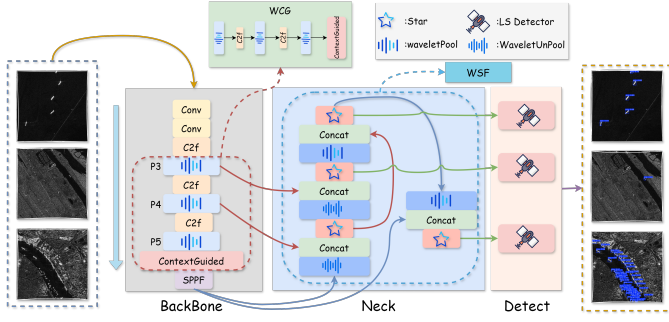


Fig. 1: Overall flow of the RSNet method.

- We introduced the Lightweight-Shared (LS) module, inspired by groupnorm, to further minimize the detection head's parameter load, thereby enhancing the overall efficiency of RSNet.
- Experiments conducted on the SSDD and the HRSID show that the proposed RSNet strikes an improved balance between lightweight design and detection performance.

## II. PROPOSED METHOD

### A. Overall Architecture

This paper introduces RSNet, a lightweight network for ship detection in SAR images, structured into backbone, neck, and head components as illustrated in Figure 1. The backbone processes the input image through the first three layers to produce feature maps, which is then enhanced by the WConv module using multiple scales of wavelet pooling to generate multi-scale feature maps (P3, P4, P5). The ContextGuided layer further enriches feature extraction by integrating contextual information. In the neck, the WSF module employs wavelet upsampling to restore spatial resolution and fuse features with the P4 map. The lightweight starnet module incorporates skip connections for deeper feature extraction, improving small object recognition. Finally, the LS Detector module concatenates features to output bounding boxes, class labels, and confidence scores for detected targets.

### B. Waveletpool-ContextGuided(WCG)

In complex backgrounds, including land structures, clutter, and coastlines, current SAR ship detectors face challenges in accurately locating ships. To achieve better performance with fewer parameters, this paper proposes the Waveletpool-ContextGuided Network (WCG).

The WCG network introduces a wavelet pooling mechanism that efficiently extracts multi-scale spatial features, reducing computational complexity while enhancing sensitivity to subtle details in complex backgrounds. This allows the network to focus on potential ship targets in noisy environments. Additionally, the context guided convolutional module integrates surrounding environmental information, significantly improving detection of small targets, especially in high-noise conditions. By leveraging contextual information, the model better distinguishes real ship targets from background noise,

enhancing localization accuracy. Below are specific descriptions of wavelet pooling and context guided convolution.

1) *Wavelet Pooling*: In the Wavelet Context-Guided Network (WCG), the WaveletPool module plays a critical role, designed to effectively extract multi-scale features from the input feature map through wavelet transforms. The output  $Y_{pool}$  of this module is defined by the following equations:

$$Y_{pool} = Conv_{2D}(Y_{C2f}) \in R^{B \times C_{out} \times H' \times W'}, \quad (1)$$

where we define the output feature map from C2f as  $Y_{C2f}$ .  $H' \times$  and  $W'$  are the dimensions of the downsampled output.  $C_{out}$  is the number of output channels of the WaveletPool layer. The filter set  $F$  used in the WaveletPool operation consists of four different convolutional kernels defined as:

$$F = \{F_{LL}, F_{LH}, F_{HL}, F_{HH}\},$$

$$F_{LL} = \begin{bmatrix} 0.5 & 0.5 \\ 0.5 & 0.5 \end{bmatrix}, F_{LH} = \begin{bmatrix} -0.5 & -0.5 \\ 0.5 & 0.5 \end{bmatrix}, \quad (2)$$

$$F_{HL} = \begin{bmatrix} -0.5 & 0.5 \\ -0.5 & 0.5 \end{bmatrix}, F_{HH} = \begin{bmatrix} 0.5 & -0.5 \\ -0.5 & 0.5 \end{bmatrix}.$$

The WaveletPool operation can be expressed as:

$$Y_{pool} = \sum_{j=1}^4 F_j * Y_{C2f}, \quad (3)$$

where  $*$  denotes the convolution operation. This operation extracts multi-scale features from the input feature map by applying each filter  $F_j$  and aggregating the results across the channel dimension.

2) *Context Guided*: The ContextGuided Block takes the input feature map and performs a series of operations, defined as:

$$Y_{CGB} = CGB(Y_{pool}). \quad (4)$$

The processing steps within the ContextGuided Block can be expressed as follows:

$$X_1 = Conv_{1 \times 1}(Y_{pool}) \in R^{B \times n \times H' \times W'}, n = \frac{C_{out}}{2}, \quad (5)$$

Then a depthwise convolution is employed to capture local features  $L$ , and another depthwise convolution with a dilation rate is applied to capture the surrounding context  $L$ :

$$L = Conv_{3 \times 3}(X_1) \in R^{B \times n \times H' \times W'}, \quad (6)$$

$$S = Conv_{3 \times 3}(X_1) \text{ with dilation rate } d. \quad (7)$$

The local features  $L$  and surrounding features  $S$  are concatenated, normalized, and activated, generating the global context feature  $F_{glo}$  through the global feature extraction module:

$$J = BatchNorm(Concat(L, S)) \in R^{B \times 2n \times H' \times W'}, \quad (8)$$

$$G = F_{glo}(J) \in R^{B \times C_{out} \times H' \times W'}. \quad (9)$$

Finally, the output of the Context Guided Block is computed by adding the input to the global context refinement output:

$$Y_{CGB} = Y_{pool} + G \quad (10)$$

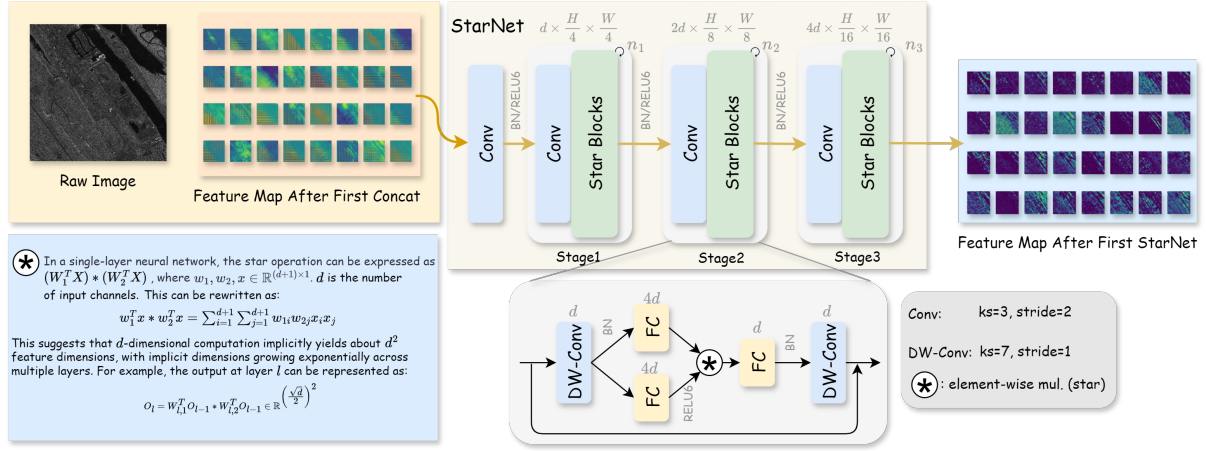


Fig. 2: Flowchart of StarNet.

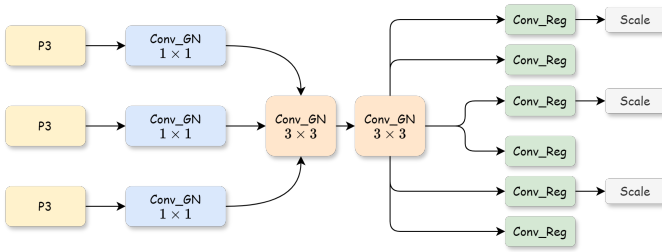


Fig. 3: The structure of LS Detector.

### C. Waveletpool-StarFusion(WSF)

Although the WCG module reduces parameters, this paper proposes the Waveletpool-StarFusion Network (WSF) to better balance parameters and model accuracy.

WaveletUnPool and StarNet enhance SAR ship detection by restoring spatial resolution and retaining rich features for improved contour recognition. StarNet utilizes depthwise separable convolutions and efficient multiplication operations for real-time applicability while effectively mitigating noise. Together, they significantly enhance performance and efficiency in ship detection.

1) *WaveletUnPool*: WaveletUnPool, in contrast, aims to restore the spatial resolution of the downsampled feature map, effectively reconstructing its original dimensions. It utilizes transpose convolution with a stride of 2, employing the same wavelet filters as described in Equation 2 to upsample the feature map back to a higher resolution.

2) *StarNet*: StarNet [17] is an advanced deep learning architecture that enhances model representation through Star Operation. By fusing features from different subspaces with element-wise multiplication at each layer, it expands implicit feature dimensions without significantly increasing parameters. Figure 2 illustrates this process in the neck section, showing the initial concatenation of the feature map before inputting it into StarNet, along with the computational flow involved.

The calculation process of Starblock is explained below. The Starblock receives an input feature map  $x_{in}$  with dimensions

$C \times H \times W$ , where  $C$  is the number of channels, and  $H$  and  $W$  are the height and width of the feature map, respectively.

- First, a depthwise convolution is applied to the input feature map  $x_{in}$ , and  $W_k$  is the convolution kernel for the  $k$ -th channel:

$$x_{in}' = DWConv(x_{in}) = \sum_{k=1}^C W_k * x_{in}, \quad (11)$$

- Next,  $1 \times 1$  convolution layers are used to transform features, producing two feature maps:

$$\begin{aligned} x_1' &= Conv_{1 \times 1}(x_{in}') = W_1 \cdot x_{in}' + b_1, \\ x_2' &= Conv_{1 \times 1}(x_{in}') = W_2 \cdot x_{in}' + b_2. \end{aligned} \quad (12)$$

The number of channels in  $x_1'$  and  $x_2'$  are both  $mlp\_ratio \times C$ , with  $mlp\_ratio = 3$ .

- Then, the first feature map undergoes ReLU6 activation, followed by element-wise multiplication with the second feature map  $x_{in}''$ , and another  $1 \times 1$  convolution layer is applied to generate a new feature map  $x^{(new)}$ :

$$x_{in}'' = \min(\max(0, x_1'), 6) \odot x_2'. \quad (13)$$

$$\begin{aligned} x^{(new)} &= DWConv2(Conv_{1 \times 1}(g(x_{in}''))) \\ &= \sum_{k=1}^C W_k^{new} * g(x_{in}'') \end{aligned} \quad (14)$$

- Finally, a residual connection is established by adding the input feature map  $x_{in}$  to the newly generated feature map, applying dropout for regularization:

$$y = x_{in} + \text{dropout}(x^{(new)}) \quad (15)$$

### D. LS Detector

The FOCS [18] shows that groupnorm enhances detection head performance in localization and classification. Shared convolutions reduce model parameters, facilitating lightweight design for resource-constrained devices. To address inconsistencies in handling targets of varying scales, we introduce a scale layer for feature adjustment. The specific structure is shown in Fig 3. These strategies lower parameters and computational load while maintaining accuracy.

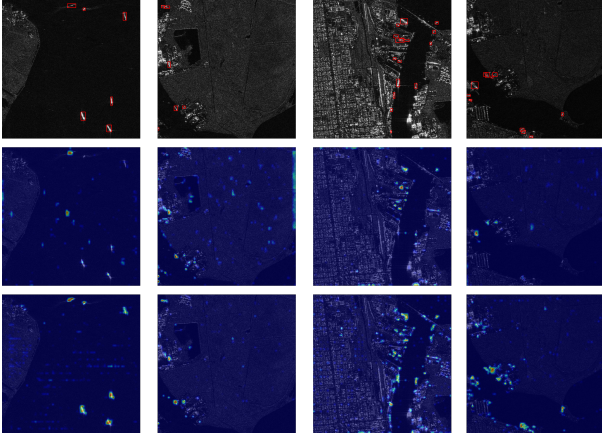


Fig. 4: The heat-map visualization results feature three rows: the first row illustrates the ground truth, the second row presents the baseline (YOLOv8n), and the third row highlights our proposed method.

TABLE I: SPECIFIC EXPERIMENTAL DETAILS

Dataset	Epochs	Optimizer	Batch	Lr0	Momentum	Weight_decay
SSDD	300	AdamW	16	0.002	0.937	5e-4
HRSID	300	AdamW	16	0.002	0.937	5e-4

### III. EXPERIMENT

#### A. Datasets

To evaluate the performance of our model, we utilized two publicly available SAR remote sensing datasets: SSDD [19] and HRSID [20]. The SSDD dataset consists of 1160 images, with 928 allocated for training and 232 for testing, as outlined in the original publication. In the case of the HRSID dataset, we adhered to the official partitioning, employing 3642 images for training and 1962 for testing purposes.

#### B. Training Details

Our experiments were conducted on a system running Ubuntu 20.04, equipped with an Intel Xeon Silver 4210R CPU and a Nvidia GeForce Tesla V100 16G. The specific experimental details are shown in Table I.

#### C. Evaluation Metrics

To evaluate the proposed model's performance, we used mean average precision at IoU = 0.5 ( $mAP_{.50}$ ) and IoU = 0.5:0.05:0.95 ( $mAP_{.50:.95}$ ), along with the number of parameters (Params) and giga floating-point operations per second (GFLOPs). The mAP metrics assess detection accuracy, while Params and GFLOPs indicate parameters and computational complexity.

TABLE II: ABLATION EXPERIMENTS ON HRSID

WCG	WSF	LS	$mAP_{.50}(\%)$	$mAP_{.50:.95}(\%)$	Params(M)	FLOPs(G)
×	×	×	91.1	66.9	3.01	8.1
✓	×	×	91.2	66.5	2.43	7.4
✓	✓	×	91.1	65.8	2.13	6.8
✓	✓	✓	91.2	67.6	1.49	5.1

TABLE III: COMPARISON EXPERIMENTS ON HRSID

Method	$mAP_{.50}(\%)$	$mAP_{.50:.95}(\%)$	Params (M)	FLOPs (G)
Faster R-CNN-FPN	72.0	46.5	41.35	134
RetinaNet	78.9	53.6	36.33	128
YOLOv6n	88.2	62.8	4.23	11.8
YOLOv7-tiny	85.4	57.2	6.01	13.2
YOLOv8n	91.1	66.9	3.01	8.1
YOLOV11n	89.7	65.8	2.59	6.4
Yue et al. [21]*	91.1	66.5	43.42	-
CPoints-Net [22]*	90.5	-	18.64	102.2
FEPS-Net [23]*	90.7	65.7	37.31	-
BL-Net [24]*	88.67	-	47.81	-
FBUA-Net [25]*	90.3	-	36.54	-
CS <sup>n</sup> Net [26]*	91.2	60.6	12.2	21.7
Ours	<b>91.2</b>	<b>67.6</b>	<b>1.49</b>	<b>5.1</b>

\* Denotes data obtained from their papers

TABLE IV: COMPARISON EXPERIMENTS ON SSDD

Method	$mAP_{.50}(\%)$	$mAP_{.50:.95}(\%)$	Params (M)	FLOPs (G)
Faster R-CNN-FPN	94.0	64.0	41.35	134
RetinaNet	90.2	60.0	36.33	128
YOLOv6n	96.9	71.2	4.23	11.8
YOLOv7-tiny	96.4	66.5	6.01	13.2
YOLOv8n	98.2	<b>73.1</b>	3.01	8.1
YOLOV11n	98.0	72.0	2.59	6.4
Yue et al. [21]*	95.7	64.8	43.42	-
CPoints-Net [22]*	96.3	-	18.64	102.2
FEPS-Net [23]*	96.0	73.1	37.31	-
BL-Net [24]*	95.25	-	47.81	-
FBUA-Net [25]*	96.2	-	36.54	-
CS <sup>n</sup> Net [26]*	97.1	64.9	12.2	21.7
Ours	<b>98.4</b>	<b>72.5</b>	<b>1.49</b>	<b>5.1</b>

\* Denotes data obtained from their papers

#### D. Ablation Experiments

To validate the effectiveness of the module, we conducted ablation experiments on the HRSID dataset, as shown in Table II. Then, to further validate the model's ability to perceive real targets, we conducted feature visualization experiments, and the results are shown in Fig. 4, where our model focuses on observing real targets while minimizes the influence of the surrounding noise.

#### E. Comparison Experiments

We selected several representative object detectors, including the classic two-stage Faster R-CNN-FPN, one-stage RetinaNet, and YOLOv6n, YOLOv7-tiny, YOLOv8n and YOLOV11n. Additionally, we compared algorithms specifically designed for target detection in SAR images. The experimental results, presented in Tables III and IV, demonstrate that our algorithm effectively balances parameter quantity and performance, outperforming other methods.

### IV. CONCLUSIONS

This paper introduces RSNet, a lightweight network for SAR ship detection that enhances accuracy and efficiency through innovative architecture. The WCG structure improves performance with fewer parameters, while the WSF network and LS module further optimize parameters. Future work will explore RSNet's application to other detection tasks and datasets, expanding its utility in remote sensing.



## REFERENCES

- [1] A. Moreira, P. Prats-Iraola, M. Younis, G. Krieger, I. Hajnsek, and K. P. Papathanassiou, "A tutorial on synthetic aperture radar," *IEEE Geosci. Remote Sens. Mag.*, vol. 1, no. 1, pp. 6–43, 2013.
- [2] M. C. Dobson, F. T. Ulaby, and L. E. Pierce, "Land-cover classification and estimation of terrain attributes using synthetic aperture radar," *Remote Sens. Environ.*, vol. 51, no. 1, pp. 199–214, 1995.
- [3] X. Bao, R. Zhang, J. Lv, R. Wu, H. Zhang, J. Chen, B. Zhang, X. Ouyang, and G. Liu, "Vegetation descriptors from sentinel-1 sar data for crop growth monitoring," *ISPRS J. Photogramm. Remote Sens.*, vol. 203, pp. 86–114, 2023.
- [4] P. Connetable, K. Conradsen, A. A. Nielsen, and H. Skriver, "Corrections to "test statistics for reflection symmetry: Applications to quad-polarimetric sar data for detection of man-made structures"," *IEEE Journal of Selected Topics in Applied Earth Observations and Remote Sensing*, 2024.
- [5] S. Baraha and A. K. Sahoo, "Synthetic aperture radar image and its despeckling using variational methods: A review of recent trends," *Signal Process.*, vol. 212, p. 109156, 2023.
- [6] S. Karimzadeh, M. Ghasemi, M. Matsuoka, K. Yagi, and A. C. Zulfikar, "A deep learning model for road damage detection after an earthquake based on synthetic aperture radar (sar) and field datasets," *IEEE J. Sel. Topics Appl. Earth Observ. Remote Sens.*, vol. 15, pp. 5753–5765, 2022.
- [7] M. G. Hashemi, E. Jalilvand, H. Alemohammad, P.-N. Tan, and N. N. Das, "Review of synthetic aperture radar with deep learning in agricultural applications," *ISPRS J. Photogramm. Remote Sens.*, vol. 218, pp. 20–49, 2024.
- [8] R. M. Asiyabi, A. Ghorbanian, S. N. Tameh, M. Amani, S. Jin, and A. Mohammadzadeh, "Synthetic aperture radar (sar) for ocean: A review," *IEEE J. Sel. Topics Appl. Earth Observ. Remote Sens.*, 2023.
- [9] G. Fracastoro, E. Magli, G. Poggi, G. Scarpa, D. Valsesia, and L. Verdoliva, "Deep learning methods for synthetic aperture radar image despeckling: An overview of trends and perspectives," *IEEE Geosci. Remote Sens. Mag.*, vol. 9, no. 2, pp. 29–51, 2021.
- [10] F. Wang, C. Chen, and W. Zeng, "Hybrid multi-scale sar ship detector with cnn-transformer and adaptive fusion loss," *IEEE Geosci. Remote Sens. Lett.*, 2024.
- [11] L. Du, L. Li, Y. Guo, Y. Wang, K. Ren, and J. Chen, "Two-stream deep fusion network based on vae and cnn for synthetic aperture radar target recognition," *Remote Sens.*, vol. 13, no. 20, p. 4021, 2021.
- [12] C. Tian, D. Liu, F. Xue, Z. Lv, and X. Wu, "Faster and lighter: A novel ship detector for sar images," *IEEE Geosci. Remote Sens. Lett.*, 2024.
- [13] Z. Zhou, J. Chen, Z. Huang, J. Lv, J. Song, H. Luo, B. Wu, Y. Li, and P. S. Diniz, "Hrle-sardet: A lightweight sar target detection algorithm based on hybrid representation learning enhancement," *IEEE Trans. Geosci. Remote Sens.*, vol. 61, pp. 1–22, 2023.
- [14] H. Chang, X. Fu, J. Dong, J. Liu, and Z. Zhou, "Mlsdnet: Multi-class lightweight sar detection network based on adaptive scale distribution attention," *IEEE Geosci. Remote Sens. Lett.*, 2023.
- [15] Y. Feng, J. Chen, Z. Huang, H. Wan, R. Xia, B. Wu, L. Sun, and M. Xing, "A lightweight position-enhanced anchor-free algorithm for sar ship detection," *Remote Sens.*, vol. 14, no. 8, p. 1908, 2022.
- [16] X. Yang, J. Zhang, C. Chen, and D. Yang, "An efficient and lightweight cnn model with soft quantification for ship detection in sar images," *IEEE Trans. Geosci. Remote Sens.*, vol. 60, pp. 1–13, 2022.
- [17] X. Ma, X. Dai, Y. Bai, Y. Wang, and Y. Fu, "Rewrite the stars," in *Proc. IEEE/CVF Conf. Comput. Vis. Pattern Recognit. (CVPR)*, 2024, pp. 5694–5703.
- [18] Z. Tian, C. Shen, H. Chen, and T. He, "Fcos: Fully convolutional one-stage object detection. arxiv 2019," *arXiv preprint arXiv:1904.01355*, 2019.
- [19] T. Zhang, X. Zhang, J. Li, X. Xu, B. Wang, X. Zhan, Y. Xu, X. Ke, T. Zeng, H. Su *et al.*, "Sar ship detection dataset (ssdd): Official release and comprehensive data analysis," *Remote Sens.*, vol. 13, no. 18, p. 3690, 2021.
- [20] S. Wei, X. Zeng, Q. Qu, M. Wang, H. Su, and J. Shi, "Hrsid: A high-resolution sar images dataset for ship detection and instance segmentation," *Ieee Access*, vol. 8, pp. 120 234–120 254, 2020.
- [21] T. Yue, Y. Zhang, P. Liu, Y. Xu, and C. Yu, "A generating-anchor network for small ship detection in sar images," *IEEE J. Sel. Topics Appl. Earth Observ. Remote Sens.*, vol. 15, pp. 7665–7676, 2022.
- [22] F. Gao, C. Cai, W. Tang, and Y. He, "A compact and high-efficiency anchor-free network based on contour key points for sar ship detection," *IEEE Geosci. Remote Sens. Lett.*, 2024.
- [23] L. Bai, C. Yao, Z. Ye, D. Xue, X. Lin, and M. Hui, "Feature enhancement pyramid and shallow feature reconstruction network for sar ship detection," *IEEE J. Sel. Topics Appl. Earth Observ. Remote Sens.*, vol. 16, pp. 1042–1056, 2023.
- [24] T. Zhang, X. Zhang, C. Liu, J. Shi, S. Wei, I. Ahmad, X. Zhan, Y. Zhou, D. Pan, J. Li *et al.*, "Balance learning for ship detection from synthetic aperture radar remote sensing imagery," *ISPRS J. Photogramm. Remote Sens.*, vol. 182, pp. 190–207, 2021.
- [25] L. Bai, C. Yao, Z. Ye, D. Xue, X. Lin, and M. Hui, "A novel anchor-free detector using global context-guide feature balance pyramid and united attention for sar ship detection," *IEEE Geosci. Remote Sens. Lett.*, vol. 20, pp. 1–5, 2023.
- [26] C. Chen, W. Zeng, X. Zhang, and Y. Zhou, "Cs n net: a remote sensing detection network breaking the second-order limitation of transformers with recursive convolutions," *IEEE Trans. Geosci. Remote Sens.*, 2023.